Transactions of Tianjin University (2022) 28:358–373
https://doi.org/10.1007/s12209-022-00336-9

REVIEW

Review on Metallization Approaches for High-Efficiency Silicon Heterojunction Solar Cells

Yulian Zeng[1] · Chen-Wei Peng[1,2] · Wei Hong[3] · Shan Wang[3] · Cao Yu[2] · Shuai Zou[1,3] · Xiaodong Su[1]

Received: 29 June 2022 / Revised: 10 July 2022 / Accepted: 17 August 2022 / Published online: 30 August 2022

Abstract

Crystalline silicon (c-Si) heterojunction (HJT) solar cells are one of the promising technologies for next-generation industrial high-efficiency silicon solar cells, and many efforts in transferring this technology to high-volume manufacturing in the photovoltaic (PV) industry are currently ongoing. Metallization is of vital importance to the PV performance and long-term reliability of HJT solar cells. In this review, we summarize the development status of metallization approaches for high-efficiency HJT solar cells. For conventional screen printing technology, to avoid the degradation of the passivation properties of the amorphous silicon layer, a low-temperature-cured (< 250 ℃) paste and process are needed. This process, in turn, leads to high line/contact resistances and high paste costs. To improve the conductivity of electrodes and reduce the metallization cost, multi-busbar, fine-line printing, and low-temperature-cured silver-coated copper pastes have been developed. In addition, several potential metallization technologies for HJT solar cells, such as the Smart Wire Contacting Technology, pattern transfer printing, inkjet/FlexTrailprinting, and copper electroplating, are discussed in detail. Based on the summary, the potential and challenges of these metallization technologies for HJT solar cells are analyzed.

Keywords Silicon solar cells · Passivating-contact · Heterojunction · Metallization · Electrode

Introduction

In recent years, passivating-contact solar cells have become the focus of the photovoltaic (PV) industry due to their remarkable efficiency potential [1]. According to the prediction of the latest International Technology Roadmap for Photovoltaic (13th edition, 2022), passivating-contact silicon heterojunction (HJT, sometimes referred to as SHJ) solar cells and other passivating-contact solar cells are rapidly expanding their market share, occupying more than 75% by 2032 [2]. The tunneling-oxide passivating-contact (TOPCon) solar cell is a powerful competitor of the HJT solar cell because its fabrication process can be upgraded on the existing PERC production line, minimizing equipment and facility costs. However, new factories usually choose the HJT solar cell technology mainly because of the following reasons: (1) HJT solar cells have a high open-circuit voltage and conversion efficiency and excellent bifaciality factor [3]. (2) HJT solar cell fabrication is a simple (few process steps) and low-temperature process, which is very beneficial for large and thin silicon wafers. (3) HJT solar cells have a low-temperature coefficient, resulting in higher energy yields compared to other silicon solar cells. (4) The symmetrical structure of HJT solar cells makes them highly adaptable to thin silicon wafers, which will be a potential cost advantage for the industrialization of HJT solar cells [3–5]. For example, HJT solar cells with a thickness of ~ 90 μm have been reported by Meyer Burger and Panasonic [6, 7].

Traditionally, HJT solar cells use a-Si:H (i/p) and a-Si:H (i/n) stacks to passivate dangling bonds on two surfaces of a wafer and form a passivating-contact, which is the most successful passivating-contact structure [8, 9]. The HJT solar

Yulian Zeng and Chen-Wei Peng have contributed equally to this work.

✉ Shuai Zou
szou@suda.edu.cn

✉ Xiaodong Su
xdsu@suda.edu.cn

[1] School of Physical Science and Technology, Jiangsu Key Laboratory of Thin Films, Soochow University, Suzhou 215006, China

[2] Suzhou Maxwell Technologies Co., Ltd., Suzhou 215200, China

[3] Suzhou Isilver Materials Co., Ltd, Suzhou 215129, China

cell technology involves two different cell structures: front emitter and rear-emitter. Between the two, rear-emitter HJT solar cells have become the mainstream HJT technology. A highly transparent conductive oxide (TCO) with relatively low conductivity requirements can be applied on the front side, resulting in a high current density [3]. Different from c-Si homojunction solar cells, HJT solar cells require a low-temperature process. This is because the hydrogen evolution from a-Si:H thin films will significantly occur when the temperature exceeds 200 ℃, which could dramatically deteriorate the passivation quality of dangling bonds on c-Si surfaces [8]. Consequently, a low-temperature metallization process is necessary for HJT solar cells.

As a well-established metallization technique, the screen printing technology is still the most commonly used metallization approach for HJT solar cell fabrication. In this technique, silver (Ag) pastes play a crucial role in contact formation and are also a core factor affecting the cost of HJT solar cells. For HJT solar cells, low-temperature-cured Ag pastes are necessary to form contact electrodes on the TCO layer, and their thermal curing temperature is usually below 250 ℃. In general, the line resistivity of a low-temperature-cured electrode is a factor of 2–3 higher than that of a high-temperature-sintered electrode [9]. To reduce the line resistance (R_{line}), the electrodes of HJT solar cells require more Ag content and a higher aspect ratio than those of other c-Si solar cells. In addition, the price of low-temperature-cured Ag pastes is > 10% higher than that of the traditional high-temperature sintered Ag pastes [10]. The high metallization cost is currently one of the most pressing challenges hindering the industrial scale expansion of HJT solar cells. In this review, we summarize the development status of the screenprinting technology for HJT solar cells, mainly including screenprinting low-temperature-cured Ag paste and low-temperature-cured Ag-coated copper (Cu) paste technologies. In addition, we review several potential metallization technologies, such as Smart Wire Contacting Technology (SWCT), pattern transfer printing (PTP), inkjet/FlexTrail printing, and Cu electroplating, to summarize their progress.

HJT Solar Cells

As one of the most promising passivating-contact technologies, silicon HJT solar cells have attracted significant attention due to their high conversion efficiency and lean process sequence. Recently, averaged HJT solar cell efficiencies of more than 25% have been reported by many research institutions and companies [4, 11, 12]. A milestone with a certified efficiency of 26.5% based on a full M6 area (274.3 cm^2) *n*-type wafer has been reported by LONGi [13]. HJT solar cells have an excellent open-circuit voltage (V_{oc}) of up to 750 mV and a very high fill factor (FF) of more than 85%, which is due to the superior interface passivation and perfect passivating-contact architecture. However, the short-circuit current density (J_{sc}) of HJT solar cells is lower than that of other silicon solar cells and even that of conventional aluminum back surface field (Al-BSF) solar cells. This is not only because of the wide bandgap of the amorphous-silicon/monocrystalline-silicon HJT structure but also due to the parasitic optical absorption losses in intrinsic and doped a-Si:H layers, especially in the uppermost front-surface field layer. To mitigate the effects of low J_{sc}, the HJ-IBC (HJT interdigitated back contact) architecture has long been known and developed [14–17] and has attracted significant attention due to the record-high efficiency of 26.7% achieved by Kaneka [18].

Figure 1a shows the typical process steps of rear-emitter HJT solar cells and structural sketches of monofacial HJT, bifacial HJT, and HJ-IBC solar cells [3]. N-type c-Si substrates are usually used as absorbers for HJT solar cells due to their higher carrier life time and lower sensitivity toward light-induced degradation compared to p-type c-Si substrates [19]. A 5–10 nm intrinsic amorphous silicon (i-a-Si:H) layer was deposited on both sides of a textured and cleaned c-Si substrate as a transition layer to passivate dangling bonds on the c-Si surface [5, 20]. Then, 5–10 nm *p*-doped and 8–15 nm *n*-doped a-Si:H layers were deposited on the front and rear sides, respectively, to provide carrier selectivity. Afterward, TCOs were deposited on both sides for the lateral charge transport to electrodes. A band diagram of the standard HJT solar cell is sketched in Fig. 1b [21].The i-a-Si:H film, as a buffer layer, enables a low c-Si surface recombination via excellent chemical passivation [22–24]. The *n*- and *p*-type-doped a-Si:H films were deposited on top of the buffer layers to form electron and hole selective contact with the c-Si absorber and TCOs, which is due to the proper work function difference between the doped a-Si:H and c-Si absorbers [25, 26]. Recently, to reduce parasitic absorption, doped microcrystalline/nanocrystalline silicon (μ/nc-Si:H) has been proven to be a promising alternative to the commonly used doped a-Si:H in the PV industry [27, 28]. Compared to a-Si:H, μ/nc-Si:H has a higher doping efficiency and optical band gap, which is beneficial for improving the *FF* and J_{sc} of HJT solar cells [28, 29]. In addition, μ/nc-Si:H can suppress the Schottky-barrier effect between *p*-doped a-Si:H and TCO(n) via the percolation path (Fig. 1c) [27, 30]. A schematic diagram of a recent state-of-the-art rear-emitter HJT solar cell featuring μ/ncc-Si:H layers as carrier-selective contacts is shown in Fig. 1d [30].

As the last step in the manufacturing process, electrode metallization has been a major efficiency-limiting and cost-determining step of HJT solar cells. The power conversion efficiency (η) of solar cells is calculated according to Eq. 1:

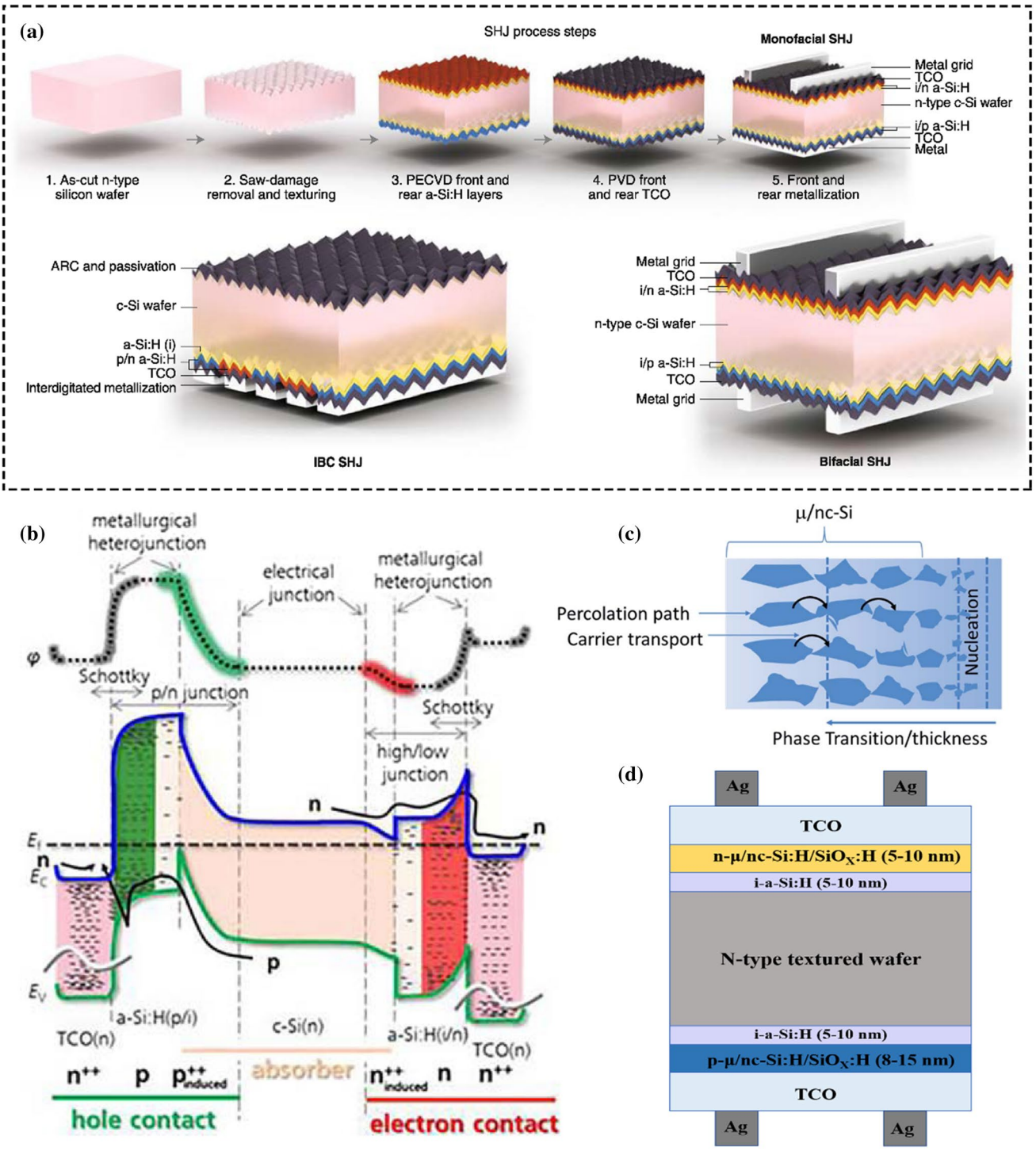

Fig. 1 **a** Typical process steps of rear-emitter HJT solar cells and structural sketches of monofacial HJT, bifacial HJT, and HJ-IBC solar cells. Reproduced with permission from Ref. [3]. Copyright© 2019 Springer Nature. **b** Band diagram of the standard HJT solar cell. Reproduced with permission from Ref. [21]. Copyright© AIP Publishing. **c** Schematic of the carrier transport mechanism in μ/nc-Si:H films. Reproduced with permission from Ref. [30]. Copyright © 2021 The Author(s). **d** Schematic diagram of a recent state-of-the-art rear-emitter HJT solar cell featuring μ/ncc-Si:H layers as carrier-selective contacts

Table 1 Summary of the key parameters of published representative HJT solar cells using various metallization technologies

Metallization	Area (cm^2)	V_{oc} (mV)	J_{sc} (mA/cm^2)	FF (%)	η (%)	Affiliation
Low-temperature-cured Ag paste	101.8	750	39.5	83.2	24.7	Panasonic [9]
	244.45	747	39.55	84.98	25.11	Hanergy [11]
	154.83	710	35.81	71.91	18.26	CAS [41]
	245.7	~734.8	~37.31	~78.8	~21.7	Fraunhofer[a] [59]
Low-temperature-cured Ag-coated Cu paste	245.7	~733.5	~36.9	~79.2	~21.6	Fraunhofer[a] [59]
	/	BL + 0.1	BL-0.03	BL-0.2	BL + 0.02	iSilverMaterials[b][60]
SmartWirecontacting technology	242.32	739	39.45	82.7	24.02	Meyer Burger [66]
Inkjet printing	245.7	733.8	38.7	81.6	23.1	Fraunhofer [59]
FlexTrail printing	245.7	737.4	39.2	82.1	23.7	Fraunhofer [59]
Cu electroplating	159	738	40.8	83.5	25.1	Kaneka [24]
	274.5	746	40.23	85.08	25.54	Maxwell/SunDrive [12]
	4	728	39.15	78.6	22.4	CSEM [73]
	243.36	717	35.4	74	18.8	UNSW [74]
	161.29	728.1	38.82	77.82	22.0	SIMIT [76]
	6.25	718	36.1	78.0	20.2	Fraunhofer [78]

[a]The data are extracted from a box diagram of electrical parameters

[b]*BL* baseline

$$\eta = \frac{P_{max}}{P_{in}} = \frac{FF \times J_{sc} \times V_{oc}}{P_{in}} \tag{1}$$

where P_{max} is the maximum power output, P_{in} is the incident light power density. Hence, η is mainly determined by three factors: FF, J_{sc} and V_{oc}.

The FF is influenced by series resistance (R_s) and shunt resistance (R_{sh}), described by Eq. 2 [31]:

$$\mathrm{FF} = \mathrm{FF}_0\left(1 - R_s\frac{J_{sc}}{V_{oc}}\right)\left(1 - \frac{1}{R_{sh}}\frac{V_{oc}}{J_{sc}}\right) \tag{2}$$

where FF_0 is the ideal FF without parasitic resistances, which is free from losses owing to the series resistance and recombination in the space charge region [32]. R_s consists of gridline, contact, emitter, and base resistances and has a significant impact on the FF [32]. Such an FF value of HJT solar cells is mainly limited by the low conductivity of silver grids produced by screen printing of pastes necessarily designed to cure at low temperatures [33].

The characteristic between the current density and voltage is expressed as Eq. 3 [34]:

$$\begin{aligned} J = {} & J_L - J_{01}\left(\exp\left(\frac{qV + JR_s}{n_1 kT}\right) - 1\right) \\ & - J_{02}\left(\exp\left(\frac{qV + JR_s}{n_2 kT}\right) - 1\right) - \frac{qV + JR_s}{R_{sh}} \end{aligned} \tag{3}$$

where J_{01} is the saturation current density caused by the recombination of electron-hole pairs in the emitter and base regions; J_{02} is the recombination current density in the space charge region, n is the ideality factor of the solar cell; J_L is the photocurrent, and q is the elemental charge. Considering the superior passivation performance of the HJT architecture, the saturation current density due to the recombination is much lower than that of other homojunction solar cells. Therefore, in the metallization step, the shading area of electrode grids, which is determined by the linewidth and aspect ratio, is an important factor affecting the J_{sc} of HJT solar cells. V_{oc} is mainly affected by the temperature and damage to the TCO layer during the metallization process [8, 35].

In addition, approximately 20% of the manufacturing costs of HJT solar cells currently originate from metallization, including the Ag paste and screen [36]. To improve photoelectric performance and reduce the manufacturing cost, various metallization technologies have been developed in the PV industry. Table 1 summarizes the key parameters of published representative HJT solar cells using various metallization technologies. In the next section, we will review the development status of several major metallization approaches for HJT solar cells.

Metallization Approaches

Screen Printing Technology

Screen printing is the most widely used contact formation technique for industrial c-Si solar cells due to its high productivity, high reliability, easy handling, and cost efficiency. The evolution of the linewidth (finger width, W_f) over the

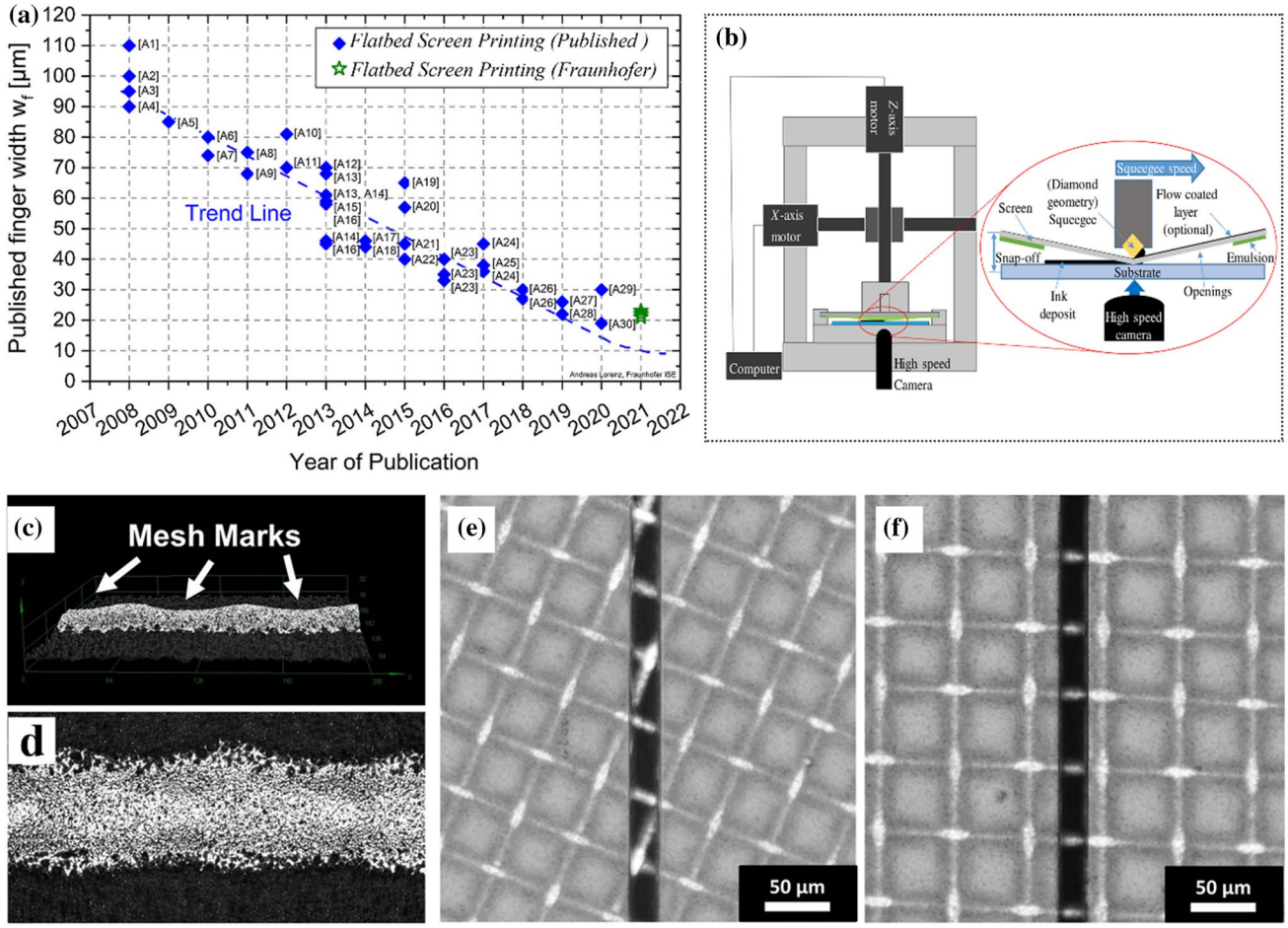

Fig. 2 **a** Evolution of the linewidth obtained with screen printing over the last 15 years [37]. **b** Schematic of a typical screen printer setup [38]. **c** Top view and **d** side view of mesh marks along screen-printed fingers due to the regular wire pattern within the finger openings in the screen [37]. **e** Conventional fine-line mesh screen with a mesh angle of 22.5° [37]. **f** Knotless screen with a mesh angle of 0° [37]. **a**, **c**, **d**, **e**, and **f** were reproduced with permission from Ref. [37]. Copyright© 2022 Elsevier. **b** was reproduced with permission from Ref. [38]. Copyright© 2019 The Author(s)

last 15 years obtained with screen printing in the PV industry is shown in Fig. 2a [37]. As can be seen, the speed of the line width improvement has been spectacular. At present, the average finger width W_f has been constantly reduced down to approximately 25 µm in industrial production lines and below 20 µm in R&D laboratories. In screen printing, pressure is applied with a squeegee to transfer metal-based pastes through a screen with a pattern to the solar cell surface to form a patterned contact electrode, as shown in Fig. 2b [38]. However, a further reduction in the screenprinting linewidth to approximately or less than 20 µm poses new challenges with respect to the screen, paste, and printing processes and quality assurance [37]. The most common case for screen-printing ultra narrow fingers leads to disruptions in the finger geometry (Fig. 2c, d) [37], finger interruptions, and alignment deviations. In the development of screen technology, the knotless screen technology has recently attracted attention due to its ability to effectively reduce mesh marks and increase the paste transfer capability, resulting in a lower mean lateral finger resistance than conventional fine-line mesh screens (Fig. 2e) and enabling an ultrafine contact [37]. As shown in Fig. 2f, a knotless screen has a mesh angle of 0° with respect to grid fingers [37]. Metal-based pastes are another important aspect that enables a high-precision printing of fine-line grids and are also an important factor that affects the electrical performance and reliability of c-Si solar cells. The following section focuses on low-temperature-cured Ag pastes and Ag-coated Cu pastes for HJT solar cells.

Low-Temperature-Cured Silver Paste

The cross-sectional SEM images of electrodes fabricated using high-temperature sintered Ag pastes and low-temperature-cured Ag pastes are shown in Fig. 3a, b, respectively

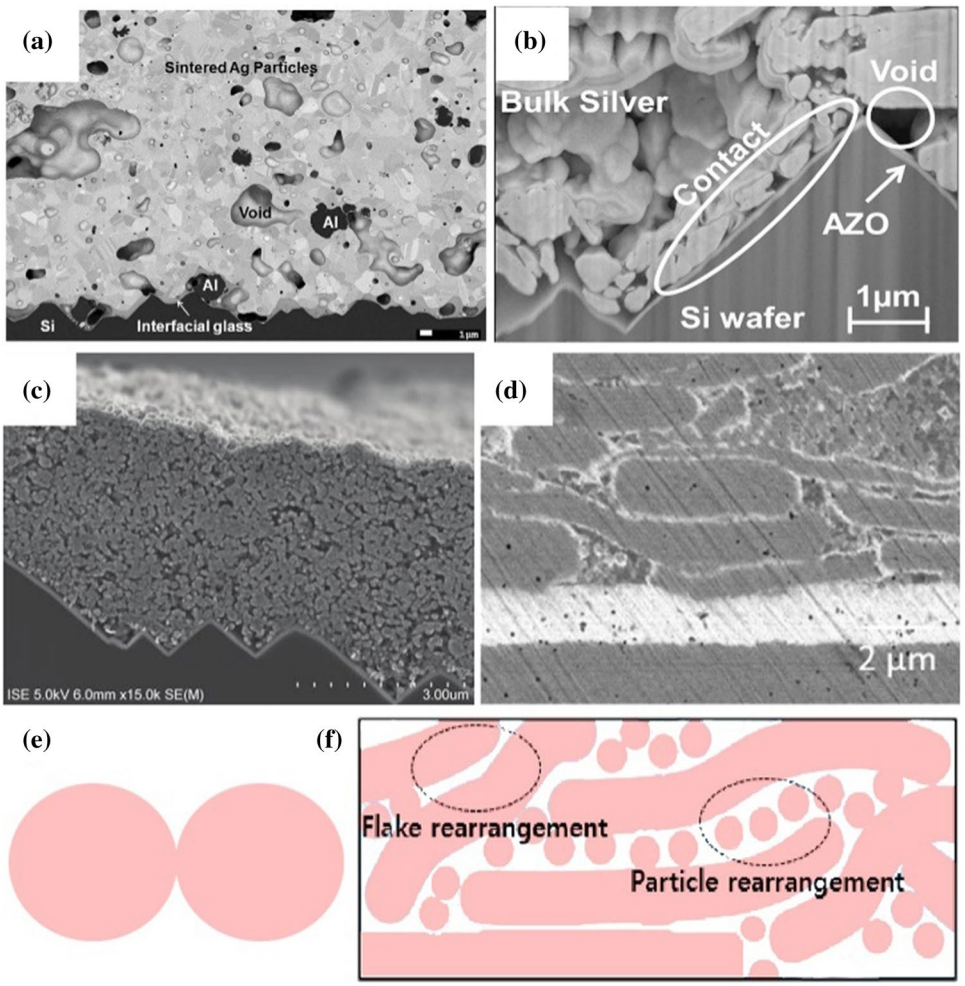

Fig. 3 Cross-sectional SEM images of electrodes fabricated using **a** high-temperature sintered Ag paste. Reproduced with permission from Ref. [39]. Copyright© 2015 AIP Publishing LLC., and **b** low-temperature-cured Ag paste. Reproduced with permission from Ref. [40]. Copyright© 2013 WIP • Sylvensteinstr. Cross-sectional SEM images of the low-temperature-cured electrodes obtained with pastes: **c** Ag nanoparticle powers. Reproduced with permission from Ref. [43]. Copyright© 2020 The Author(s), and **d** mixing powers of micronflakes and Ag nanoparticles [44]. **e** Schematic diagram of the Ag nanoparticle contact. **f** Schematic diagram of the Ag nanoparticle and micronflakes contact [44]. **e**, **f** was reproduced with permission from Ref. [44]. Copyright© 2020 The Author(s)

[39, 40]. The high-temperature sintered electrode is very dense and almost becomes a whole bulk. The conductive powders of the low-temperature-cured electrode are relatively dispersed, and many voids exist in the electrode bulk. A low-temperature-cured Ag paste consists of metal powders, binder resins, solvents, curing agents, and other additives [41]. Metal powders are the conductive phase, accounting for more than 90% of the paste. The resins act as the binder of metal powders and provide the adhesion of the electrode to the TCO. The solvents usually consist of short-chain hydrocarbons with low boiling points to adjust the rheological and wettability properties of pastes and are easy to burn off. The curing agents react with resin to prompt the resin polymerization [42].

Low-temperature-cured electrodes usually have a relatively high bulk resistivity, so high consumption is required to ensure an acceptable FF, resulting in high metallization costs. For low-temperature-cured Ag pastes consisting of Ag nanoparticles with high surface energy, although they are conducive to achieving curing at low temperatures, Ag nanoparticles are usually in point-to-point contact (Fig. 3c), which increases the bulk resistivity of the Ag electrode [43, 44]. It has been proven that the combination of Ag micronflake powers and Ag nanoparticle powders can significantly improve the conductivity of Ag electrodes cured at low temperatures [44, 45]. As shown in Fig. 3d, adding an appropriate proportion of Ag micronflakes into a paste can increase the contact area, and the rearrangement of nanoparticles between micronflakes increases the density of the Ag electrode [44, 46]. The schematic diagrams of contact mechanisms corresponding to the above two cases (Fig. 3c, d) are depicted in Fig. 3e, f. During the curing process of low-temperature silver pastes, low-boiling-point solvents gradually burn off along with the shrinkage and cross-linking of the resin, and the diffusion of atoms on the surface of Ag nanoparticles will facilitate the connection of Ag microparticles [42, 47]. Finally, a dense conductive mesh was formed by a large thermodynamic driving force provided by the resin and molten silver nanoparticles [41, 47]. Therefore, the effect of the organic composition in the paste on the conductivity of the low-temperature-cured electrode is also critical. To increase the conductivity of electrodes,

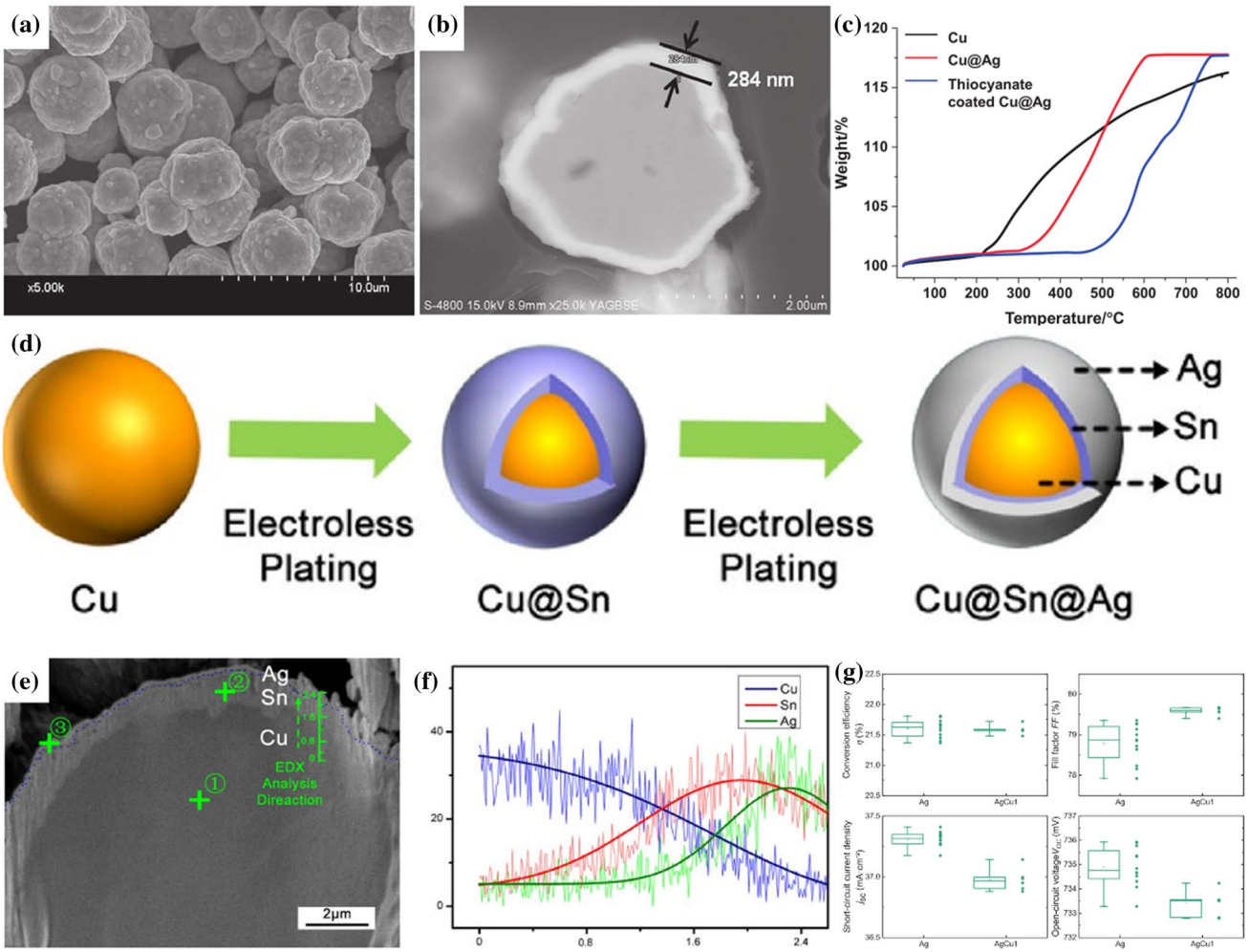

Fig. 4 **a** SEM image of thiocyanate-coated Cu@Ag particles. **b** Cross-sectional BSE image of Ag-coated Cu particles. **c** TGA graphs of the Cu particles Cu@Ag particles and thiocyanate-coated Cu@Ag particles under air conditions. **a–c** were reproduced with permission from Ref. [56]. Copyright © 2015 The Chemical Society of Japan. **d** Schematic diagram of the Cu@Sn@Ag sandwich structure. **e** Cross-sectional SEM image of the Cu@Sn@Ag particle and **f** corresponding EDX line-scan analysis. **d–f** were reproduced with permission from Ref. [57]. Copyright© 2019, Springer Science Business Media. **g** *I–V* characteristics of HJT solar cells metallized separately by Ag-coated Cu paste and Ag paste screenprinting. Reproduced with permission from Ref. [59]. Copyright© 2019The Author(s)

the amount of resin should be appropriately reduced under the condition of ensuring adhesion. An optimal combination of resins, solvents, curing agents, and other additives are desired [42], and organic components need to be burned off as low as possible below the curing temperature [41, 47]. According to a report from Fusion New Material [48], a bulk resistivity of ~ 4.5 Ω cm could be achieved in 2022.

Low-Temperature-Cured Silver-Coated Copper Paste

Ag powders account for approximately 98% of the cost of low-temperature-cured Ag pastes, which restricts the decrease in the paste cost. Copper has an electrical conductivity similar to that of Ag and is much less expensive and more abundant than Ag, making it an ideal alternative metal for Ag. However, Cu is less resistant to oxidation [49, 50], making it difficult to maintain high electrical conductivity for long periods of time [51]. To overcome this problem, Ag-coated Cu paste technology has recently attracted extensive attention in the field of HJT technology.

The coating quality of Ag-coated Cu powders is very important to the performance of Ag-coated Cu pastes. Electroplating [52], electroless plating [53, 54], and vacuum processes [55] are commonly used for powder coating processes. The electroless plating process to fabricate Ag-coated Cu powders is widely used due to its simplicity, low cost, and high quality. Shin et al. [56] synthesized thiocyanate-modified Ag-coated Cu particles with excellent oxidation resistance via electroless plating. As shown in Fig. 4a, tiny agglomerates of the β-CuSCN layer

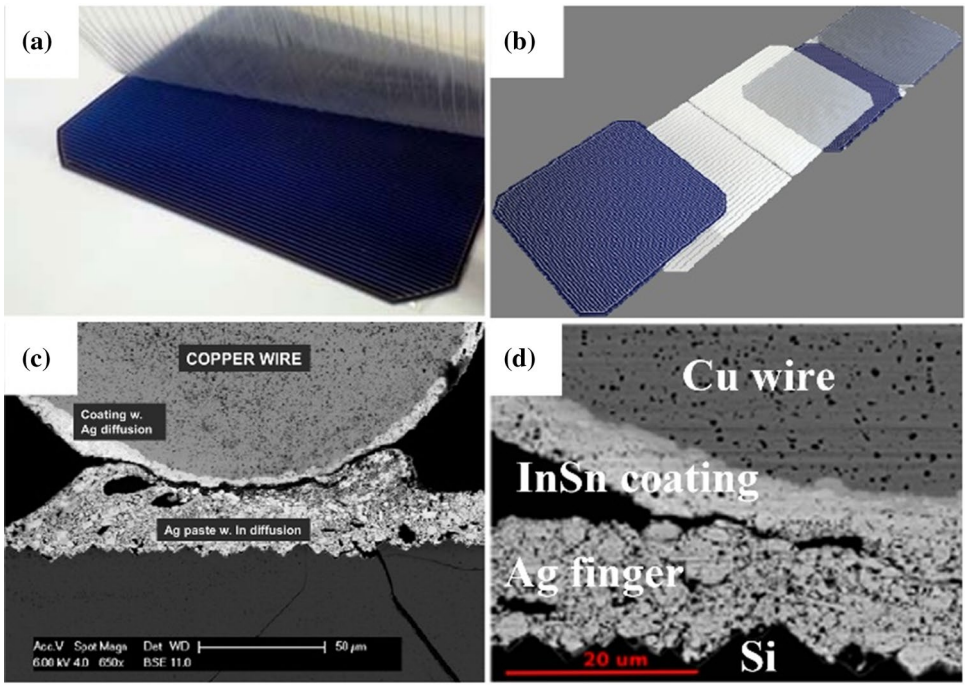

Fig. 5 **a** Picture of a SmartWire foil on a busbar-less cell. **b** Schematic diagram of automated SmartWire cell interconnection. **c** and **d** Cross-sectional BSE images of the contact point between the InSn-coated Cu wire and Ag finger. Reproduced with permission from Ref. [64]. Copyright© 2014 WIP • Sylvensteinstr

plugged the pores on the surface of Ag-coated Cu particles, and the Cu cores were uniformly wrapped by an Ag shell of approximately 300 nm (Fig. 4b). Compared with unmodified Ag-coated Cu particles, the oxidation temperature of thiocyanate-modified Ag-coated Cu particles increased by 150 ℃ (Fig. 4c). To address the transient liquid phase bonding of low-temperature pastes, Liu et al. [57] proposed a Cu@Sn@Ag sandwich structure, whose schematic diagram is shown in Fig. 4d. The cross-sectional SEM image and EDX line-scan analysis of the Cu@Sn@Ag particle (Fig. 4e, f) illustrate that the thicknesses of the Sn and Ag coatings on the Cu particles are 1.2 and 0.4 µm, respectively. Sun et al. [58] used ethylenediamine as the Ag complexing agent and adjusted the pH value of the plating solution to prepare Ag-coated Cu micronflakes with smooth surfaces. The prepared Ag-coated Cu micronflake powders exhibited a resistivity of 3.9×10^{-4} Ω·cm. Schube et al. [59] compared the electrical characteristics of HJT solar cells metallized separately using Ag-coated Cu paste and Ag paste screenprinting. As shown in Fig. 4g, the Ag-coated Cu paste group shows a conversion efficiency similar to that of the Ag paste group, and the high FF caused by a low grid resistance is the main advantage of the Ag-coated Cu paste with a high amount of Ag fill material. Hong [60] reported that approximately 0.09% efficiency loss was obtained on SHJ cells using the Ag-coated Cu paste (HAC539-T3) instead of the front and rear finger Ag pastes of the baseline. According to the report from Toyo Aluminum K.K., the HJT mini-module using the Ag-coated Cu paste (THA-F08C4) has a power degradation of less than 5% after TC 200 [61]. In particular, Ag-coated Cu pastes are not suitable for silicon homojunction solar cells due to the dewetting behavior of the Ag shell at high temperatures [62].

Some problems still need to be solved or improved for screen printing low-temperature-cured metal paste technology. First, the electrodes of HJT solar cells fabricated by screen printing low-temperature-cured metal pastes show relatively poor adhesion on TCO films. Hence, it is an important optimization direction to improve the organic composition in the paste without increasing the contact resistance. Second, due to the high resin content of the low-temperature-cured paste and the large diameter of the metal microflakes, slow printing and flooding velocities are essential to maintain the printing quality but affect the throughput. In addition, a curing time of 5–8 min is essential even with the rapid low-temperature curing process for HJT solar cells, compared to traditional PERC solar cells with a high-temperature sintering time of approximately 1 min. The long curing time usually leads to low throughput and high capital expenditures, and reliability is still a concern for rapid curing technologies.

SWCT

SWCT, as an innovative HJT solar cell interconnection process for module manufacturing, was initially proposed by Day4 Energy [63] and further developed by Meyer Burger for automated production lines [64]. The SWCT consists of Cu wires coated with a thin low-melting-point alloy (InSn/

BiSn) layer and supported by a polymer foil (Fig. 5a, b) [64]. In Fig. 5a, the diameter and gap of the wires can be as small as 70 μm and 4 mm, respectively [64]. The cross-sectional BSE images of the contact point between the coated Cu wire and Ag finger are shown in Fig. 5c, d [64]. Due to the abundant electrical contact points of every cell, the requirements for line conductance can be relaxed, and fine-line printing can be allowed while ensuring high module reliability. Busbarless technology shows prospects for ultralow Ag content with 30 mg laydown [64]. Narrow wires and fingers reduce shadow, thus improving J_{sc}. Moreover, the power loss is positively correlated with the line resistance of fingers, which increases with increasing finger length, and it is negatively related to the number of busbars [65]. The finger length is defined as half the distance from one busbar to an adjacent busbar in a standard H-pattern. The multiwire SWCT technology can significantly increase the module output power by reducing R_{line} and emitter resistivity ($R_{emitter}$). Zhao et al. [66] demonstrated a champion cell with 24.02% conversion efficiency in a pilot production line and a 60-M2 cell SWCT monofacial module with 335 W.

PTP

Fine finger technology is beneficial in reducing shading, increase I_{sc} and V_{oc}, and reduce emitter resistivity. The *FF* loss caused by the increased series resistance can be compensated by SWCT. As mentioned above, due to the limitation of the wire size, mesh, and emulsion, it is difficult for screen printing to steadily print fingers with linewidths less than 20 μm.

PTP, a contactless printing technology commercialized by Utilight, has recently received much attention due to its potential for fine and high aspect ratio metallization fingers. As shown in Fig. 6a, b, fingers smaller than 20 μm can be deposited through PTP technology [67]. Its working principle is illustrated in Fig. 6c [67]. First, a transparent polymer tape with trenches is filled with the paste using blades. The polymer tape is then placed approximately 200 μm away from the wafer, and the paste is detached from the trenches by evaporating the solvent with an infrared laser [68]. Maybury et al. [69] compared the electrical characteristics of c-Si PERC solar cells metallized via PTP and screen printing. As shown in Fig. 6d, the PTP technology shows an efficiency gain of $0.14\%_{abs}$, which is mainly contributed by the I_{sc} and V_{oc} gains. According to a report submitted by Adrian et al. [68], PTP technology could reduce the paste lay down to approximately 30 mg. Compared with its application in PERC solar cells, PTP technology is more suitable for HJT solar cells without SiN_x, and the noncontact printing manner is more conducive to the thinning wafer tendency for HJT solar cells. Nevertheless, some problems still need to be solved for the large-scale industrial application of PTP technology. As presented in Fig. 6e, f, a large number of finger interruptions occurred on single PTP-printed cells [67]. In addition, the paste tends to remain in the polymer tape, which means extra paste waste.

Inkjet Printing and FlexTrail Printing

Inkjet printing and FlexTrail printing are ultralow Ag consumption technologies utilizing a commercially available Ag nanoparticle ink. In the inkjet printing process, the ink is ejected from a pulsed voltage-controlled nozzle without touching the wafer, as shown in Fig. 7a [43]. In the FlexTrail printing process, the ink is pressed out from the lower end of a hollow glass capillary with an inner diameter of several microns, whose end is in a flexible contact with the wafer (Fig. 7b) [43].

The fingers fabricated by inkjet printing and FlexTrail printing utilizing the same Ag nanoparticle ink are shown in Fig. 7c, d [43]. As can be seen, the width of the inkjet printed finger (75 ± 1 μm) is a factor of 4.7 higher than that of the FlexTrail printed finger (16 ± 1 μm) [59]. The laydown of the latter only consumed 0.3 ± 0.1 mg on a large-area HJT solar cell with 80 front fingers, but it still achieved a conversion efficiency of 23.7%. The two ultralow Ag consumption printing technologies are expected to be breakthrough metallization technologies for HJT solar cells, but their reliability still needs further research.

Copper Electroplating

Although various low-consumption Ag technologies have been introduced above, a certain amount of Ag consumption is unavoidable. Ag-free metallization has received extensive attention from PV academic and industrial circles. As mentioned above, Cu is dozens of times cheaper than Ag, but they have similar conductivity. Cu electroplating, as an Ag-free metallization technique, plays an important role in the new metallization technologies of HJT solar cells [70]. This technology has been industrially proven for silicon homojunction solar cells [71]. Recently, Cu electroplating metallization has attracted much attention for HJT solar cell processing because it is expected to solve the current dilemma of the high cost caused by the high consumption and high price of low-temperature Ag pastes. In addition, the resistivity of the Cu-plated electrode is much lower than that of the screen-printed Ag electrode, and fine fingers can be achieved, thus further improving the conversion efficiency of HJT solar cells. Figure 8a shows the in-line electroplating equipment produced by JBAO Technology Ltd. [72]. The appearance of a Cu-electroplated HJT solar cell is shown in Fig. 8b [72]. In 2015, Kaneka announced that a 159 cm^2 HJT solar cell with a Cu grid electrode achieved 25.1% efficiency [24, 65]. In 2021, Maxwell and SunDrive [12] reported an

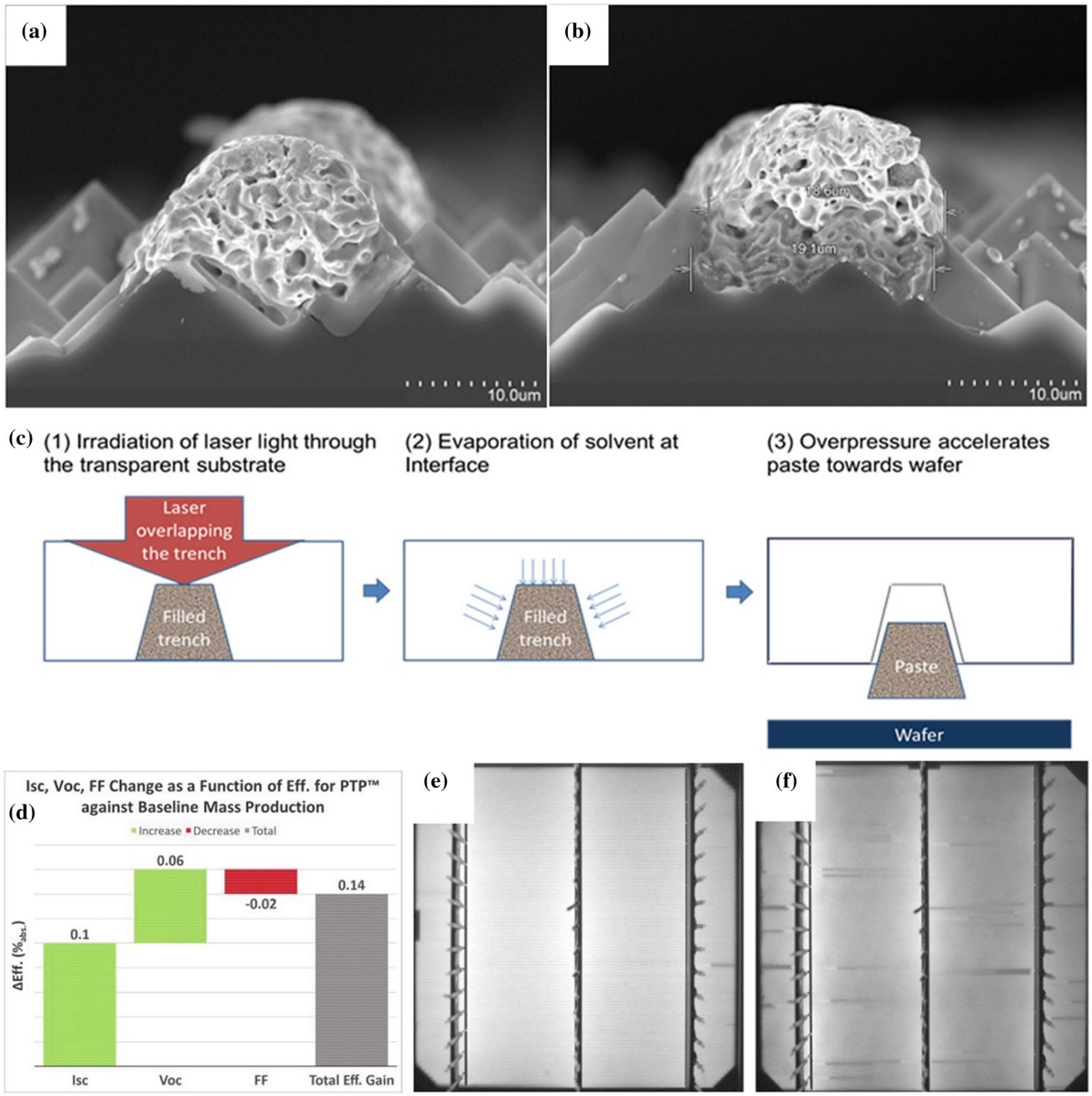

Fig. 6 **a** and **b** SEM images of a finger smaller than 20 µm deposited by PTP. **c** Schematic diagram of the working principle of PTP [67]. **d** Electrical performance gain of solar cells metallized with PTP compared to reference cells with screen printing [69]. EL images from typical c-Si solar cells metalized by **e** screen printing and **f** single PTP printing [67]. **a**, **b**, **c**, **e**, and **f** were reproduced with permission from Ref. [67]. Copyright© 2015 Elsevier. **d** was reproduced with permission from Ref. [69]. Copyright© 2019 The Author(s)

M6 HJT solar cell metallized by seed-free Cu electroplating that achieved 25.54% conversion efficiency. The Cu electroplating technology can achieve such satisfactory efficiencies mainly due to the acquisition of a narrow linewidth and low series resistance. CSEM [73] reported that an HJT solar cell with plated fingers with a linewidth of 15 µm and an aspect ratio of 1:1 can obtain a gain of J_{sc} 1.1 mA/cm^2 compared to a reference cell with Ag paste screenprinting. Moreover, the electroplated Cu electrode is close to bulk Cu [74], and its resistivity (2×10^{-8} Ω m) is similar to that of pure Cu (1.75×10^{-8} Ω m), which is several times lower than that of the screen-printed Ag electrode [73, 75], thus achieving a lower line resistance and contact resistance.

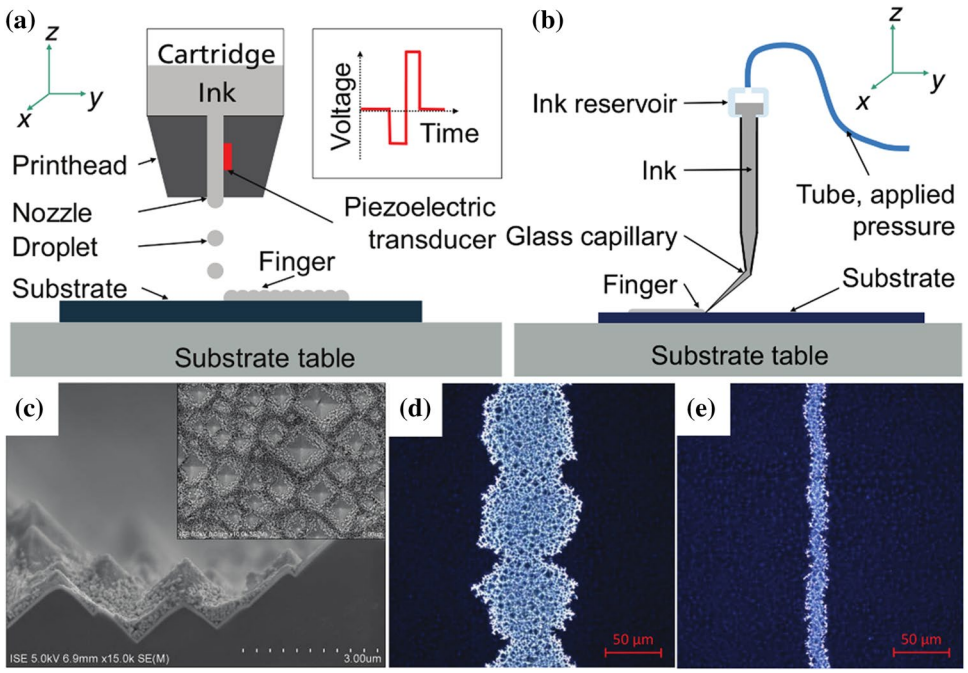

Fig. 7 Schematic diagrams of the working principle of **a** inkjet printing and **b** FlexTrail printing [43]. **c** Cross-sectional SEM image of an inkjet printed finger. Inset: corresponding top view SEM image. Microscopy images at a magnification of 50 of the fingers printed by **d** inkjet printing and **e** FlexTrailprinting [59]. **a**, and **d** were reproduced with permission from Ref. [43]. Copyright© 2020 The Author(s). **c**, **e**, and **d** were reproduced with permission from Ref. [59]. Copyright© 2019 WILEY-VCH

Although TCO films can effectively solve the carrier lateral transport problem for HJT solar cells, they bring some difficulties to the Cu electroplating metallization technique. First, a patterned mask process is required to define electrode openings. Due to the high cost of photoresists, various alternative organic and inorganic masks have been developed. Among them, dry films and resin resists exhibit a high resolution and low cost in organic-material masks [74, 76]. Yu et al. [76] reported that dry films have a good resolution of 30–50 µm. As shown in Fig. 8c, the opening trench of the dry film is nearly rectangular, and the thickness is close to 40 µm after development. Figure 8d, e shows that the cross section of the electroplated Cu finger is rectangular with a width of approximately 56 µm and a thickness of approximately 25 µm [76]. Li et al. [74] reported a resin solution (resist) obtained from a modified AZ nLOF 2035 photoresist to obtain openings without lithographic development. The development was performed in a tetramethyl ammonium hydroxide solution after baking at 110 ℃, and an approximately 20 µm line opening was obtained, as shown in Fig. 8f. Plated fingers with a width as narrow as approximately 20 µm and a height of approximately 10 µm were achieved, as shown in Fig. 8g, h. In particular, UV exposure is no longer required to use this resin. However, the removal of the organic mask will produce a large amount of wastewater, and the position of Cu fingers in contact with the organic template cannot be easily protected by the Ag/Sn layer to prevent Cu oxidation [77]. Some people have suggested that inorganic masks are highly suitable for mass production owing to their high throughput and low cost [75]. Native oxides of metals [78, 79], SiO_x [80], Al_2O_3/a-Si stacks [81], and SiO_x/SiN_x stacks [82] have been reported as favorable inorganic masking materials. For example, Hatt et al. [78] deposited Cu/Al stacks onto a TCO film via physical vapor deposition (PVD), and pattern openings were formed via etching in a sodium hydroxide solution, as shown in Fig. 8i. The finger electrodes plated by a forward/reverse pulsed current are presented in Fig. 8j, k. Second, the adhesion of an electroplated Cu electrode on TCO should be considered, which will affect the long-term reliability of the corresponding modules [78]. Li et al. [83] used an electrochemical method to reduce indium particles from tungsten-doped indium oxide films as a seed layer, and the maximum peel force of the electroplated Cu busbar reached 4.23 N [83]. Although this method provides a method to solve the low peel force of electroplated Cu electrodes, it is not economical. The research on improving the peel force of electroplated Cu electrodes is still in progress. In addition, the cumbersome process steps bring additional costs, and the long-term reliability still needs to be explored [12].

Summary and Outlook

Herein, we review the development status of metallization approaches for c-Si HJT solar cells. Although much effort has been currently performed in transferring the HJT solar cell technology to high-volume manufacturing, metallization is still one of the major factors slowing down its industrialization progress. Metallization not only affects the electrical performance and cost of HJT solar cells but also affects the long-term reliability of HJT module products.

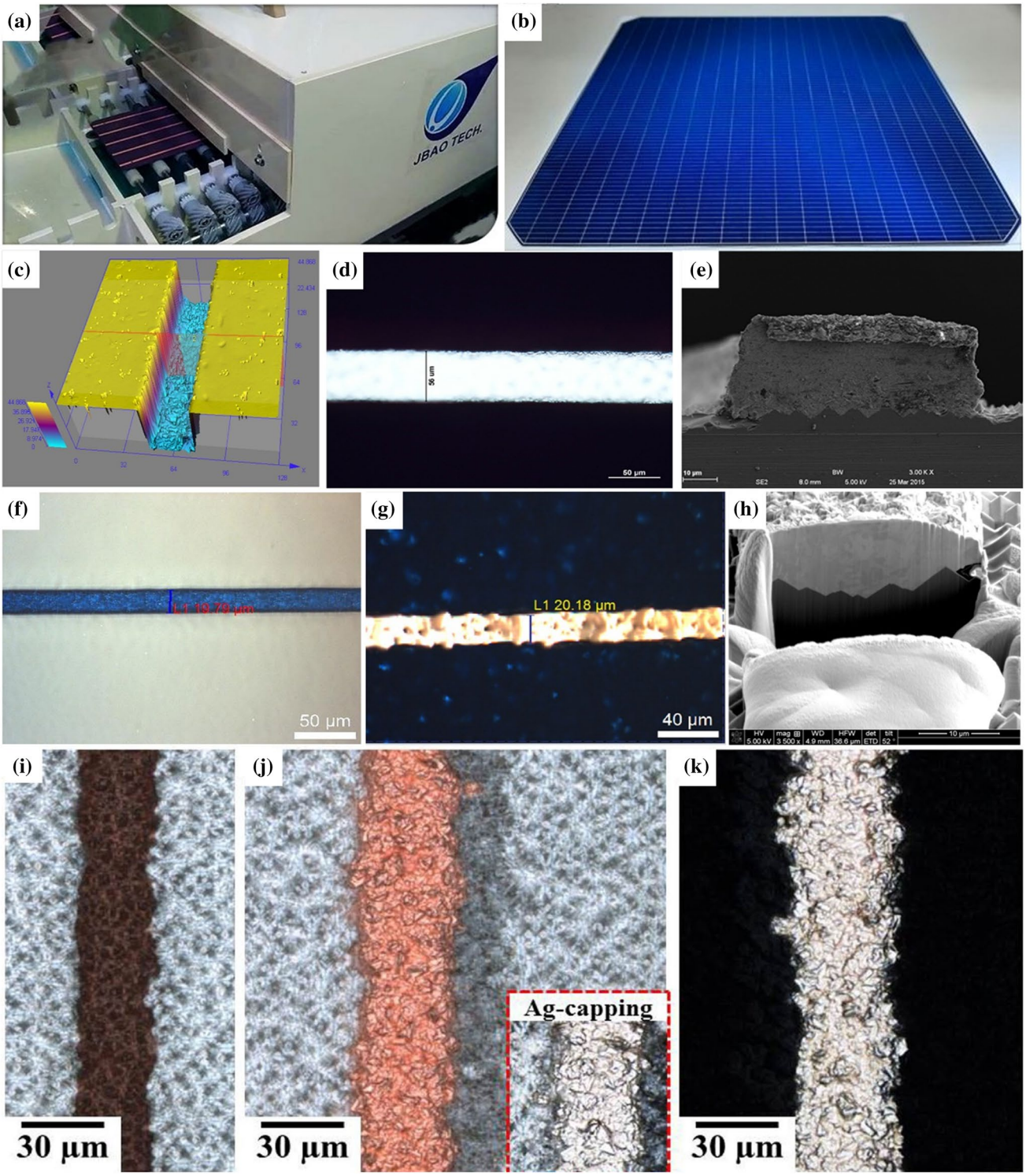

Fig. 8 **a** Electroplating equipment and **b** Cu-electroplated HJT solar cell from JBAO Technology Ltd. [72]. Microscopic images of **c** a dry film after development and **d** electroplated finger. **e** Cross-sectional SEM image of the electroplated Cu finger [76]. Microscopic images of **f** a resin obtained by modifying a photoresist after development and **g** electroplated finger, **h** FIB cross-sectional image of the electroplated Cu finger [74]. Microscopic images of **i** a finger opening on the Cu/Al stacks by inkjetprinting NaOH solution, **j** electroplated Cu finger with Ag capping, and **k** the finger after etching-back PVD layers [78]. **a**, and **b** were reproduced with permission from Ref. [72]. Copyright© JBAO Technology Ltd. **c**, **d**, and **e** were reproduced with permission from Ref. [76]. Copyright© 2017 Elsevier. **f**, **g**, and **h** were reproduced with permission from Ref. [74]. Copyright© 2015 Elsevier. **i**, **j**, and **k** were reproduced with permission from Ref. [78]. Copyright© 2019 WILEY–VCH

Among the many metallization technologies, screen printing is the most widely used in HJT solar cell manufacturing. Screens and pastes are two key materials in screen printing and have played very important roles in the impressive progress of c-Si solar cells in the past two decades. With the development of screen technology, screen-printed fingers with a width of 20–25 μm have been achieved. In addition, knotless screens have good development prospects because they support effective paste usage and fine metallization fingers. Low-temperature-cured Ag pastes have become one of the major factors restricting the cost reduction of HJT solar cells due to their high usage and price. Recently, a low-temperature-cured Ag-coated Cu paste was developed to reduce the material cost of low-temperature-cured pastes. Essentially, screenprinting technology based on low-temperature-cured pastes still needs improvement in terms of printing speed, curing time, and electrode adhesion.

To further reduce metallization costs, the industry also focuses on new metallization technologies, such as SWCT, PTP, inkjet/FlexTrailprinting, and Cu electroplating. The SWCT is an innovative interconnection technology for HJT solar cells and modules and has attracted attention for its ability to significantly reduce Ag consumption. The novel PTP technique is capable of depositing very fine metallization fingers (≤ 20 μm) with a high aspect ratio, thus significantly improving the efficiency of HJT solar cells. Nonetheless, some problems still need to be solved before large-scale applications, such as finger interruptions and extra paste waste. Inkjet printing and FlexTrail printing offer significant Ag reduction potential. Compared to the inkjet printing process, the FlexTrail printing process can achieve a finer finger width and consume less Ag ink, showing a great cost-saving potential. As an Ag-free metallization technique, Cu electroplating technology has been proven feasible in the industry. However, additional masking steps and subsequent mask-removal steps increase the manufacturing costs and complexity of HJT solar cells. Simple and low-cost mask technology has recently become a topic of increasing interest for the Cu electroplating process, which is also the key to its large-scale application in HJT solar cell manufacturing.

Although many constraints and challenges still need to be addressed, new metallization technologies should also be highlighted to disburden the current limitations of screen-printing metallization and pave the way for further efficiency increases and cost reductions in HJT solar cells and modules. Finally, the large-scale application of new metallization technologies needs to consider the long-term reliability of corresponding module products and patent risks.

Acknowledgements This work was supported by the Priority Academic Program Development of Jiangsu Higher Education Institutions (PAPD).

Conflict of interest The authors declare that they have no known competing financial interests or personal relationships that could have appeared to influence the work reported in this paper.

References

1. Chavali RVK, de Wolf S, Alam MA (2018) Device physics underlying silicon heterojunction and passivating-contact solar cells: a topical review. Prog Photovolt Res Appl 26(4):241–260. https://doi.org/10.1002/pip.2959
2. ITRPV consortium (2022) International technology roadmap for photovoltaic (ITRPV). https://www.vdma.org/viewer/-/v2article/render/50902381
3. Allen TG, Bullock J, Yang XB et al (2019) Passivating contacts for crystalline silicon solar cells. Nat Energy 4(11):914–928
4. Yoshikawa K, Yoshida W, Irie T et al (2017) Exceeding conversion efficiency of 26% by heterojunction interdigitated back contact solar cell with thin film Si technology. Sol Energy Mater Sol Cells 173:37–42. https://doi.org/10.1016/j.solmat.2017.06.024
5. Goodrich A, Hacke P, Wang Q et al (2013) A wafer-based monocrystalline silicon photovoltaics road map: utilizing known technology improvement opportunities for further reductions in manufacturing costs. Sol Energy Mater Sol Cells 114:110–135. https://doi.org/10.1016/j.solmat.2013.01.030
6. Zhao J, König M, Wissen A et al (2017) > 23% silicon heterojunction solar cells in Meyer Burger's Demo line: results of pilot production on mass production tools. In: IEEE 44th photovoltaic specialist conference. Washington, DC, pp 1752–1754. https://doi.org/10.1109/PVSC.2017.8366365
7. Mette A (2007) New concepts for front side metallization of industrial silicon solar cells. University of Freiburg, Baden-Württemberg
8. de Wolf S, Kondo M (2009) Nature of doped a-Si: H/c-Si interface recombination. J Appl Phys 105(10):103707. https://doi.org/10.1063/1.3129578
9. Taguchi M, Yano A, Tohoda S et al (2014) 24.7% record efficiency HIT solar cell on thin silicon wafer. IEEE J Photovolt 4(1):96–99. https://doi.org/10.1109/JPHOTOV.2013.2282737
10. Liu ZX (2022) HJT vs PERC+TOPCon: opportunities and challenges. In: 19th China photovoltaic academic conference. China
11. Ru XN, Qu MH, Wang JQ et al (2020) 25.11% efficiency silicon heterojunction solar cell with low deposition rate intrinsic amorphous silicon buffer layers. Sol Energy Mater Sol Cells 215:110643. https://doi.org/10.1016/j.solmat.2020.110643
12. Shen WZ, Zhao YX, Liu F (2022) Highlights of mainstream solar cell efficiencies in 2021. Front Energy 16(1):1–8. https://doi.org/10.1007/s11708-022-0816-x
13. LONGi (2022) 26.50%! LONGi sets new world record for HJT cell efficiency. WeChat official account of LONGi. https://mp.

weixin.qq.com/s/QU7e18I2uuKCo_E3Wodm-Q. https://mp.weixin.qq.com/s/QU7e18I2uuKCo_E3Wodm-Q.Accessed25June2022
14. Savin H, Repo P, von Gastrow G et al (2015) Black silicon solar cells with interdigitated back-contacts achieve 22.1% efficiency. Nat Nanotechnol 10(7):624–628
15. Zarede T, Lidjici H, Mahrane A et al (2018) 3D numerical simulation of bifacial heterojunction silicon p-type solar cell. SILICON 10(4):1745–1753. https://doi.org/10.1007/s12633-017-9664-4
16. Verlinden PJ, Aleman M, Posthuma N et al (2012) Simple power-loss analysis method for high-efficiency interdigitated back contact (IBC) silicon solar cells. Sol Energy Mater Sol Cells 106:37–41. https://doi.org/10.1016/j.solmat.2012.06.008
17. Rahman T, To A, Pollard ME et al (2018) Minimising bulk lifetime degradation during the processing of interdigitated back contact silicon solar cells. Prog Photovolt Res Appl 26(1):38–47. https://doi.org/10.1002/pip.2928
18. Bonilla RS, Hoex B, Wilshaw PR (2020) Special issue: surface and interface passivation in crystalline silicon solar cells. Sol Energy Mater Sol Cells 213:110580. https://doi.org/10.1016/j.solmat.2020.110580
19. Bivour M, Steinkemper H, Jeurink J et al (2014) Rear emitter silicon heterojunction solar cells: fewer restrictions on the optoelectrical properties of front side TCOs. Energy Procedia 55:229–234. https://doi.org/10.1016/j.egypro.2014.08.035
20. Stuckelberger M, Biron R, Wyrsch N et al (2017) Review: progress in solar cells from hydrogenated amorphous silicon. Renew Sustain Energy Rev 76:1497–1523. https://doi.org/10.1016/j.rser.2016.11.190
21. Hermle M, Feldmann F, Bivour M et al (2020) Passivating contacts and tandem concepts: approaches for the highest silicon-based solar cell efficiencies. Appl Phys Rev 7(2):021305. https://doi.org/10.1063/1.5139202
22. Panigrahi J, Komarala VK (2021) Progress on the intrinsic a-Si: H films for interface passivation of silicon heterojunction solar cells: a review. J Non Cryst Solids 574:121166. https://doi.org/10.1016/j.jnoncrysol.2021.121166
23. Olibet S, Vallat-Sauvain E, Ballif C (2007) Model for a-Si: H/c-Si interface recombination based on the amphoteric nature of silicon dangling bonds. Phys Rev B 76(3):035326. https://doi.org/10.1103/physrevb.76.035326
24. Adachi D, Hernández JL, Yamamoto K (2015) Impact of carrier recombination on fill factor for large area heterojunction crystalline silicon solar cell with 25.1% efficiency. Appl Phys Lett 107(23):233506. https://doi.org/10.1063/1.4937224
25. Bivour M, Schröer S, Hermle M (2013) Numerical analysis of electrical TCO/a-Si: H(p) contact properties for silicon heterojunction solar cells. Energy Procedia 38:658–669. https://doi.org/10.1016/j.egypro.2013.07.330
26. Khokhar MQ, Hussain SQ, Kim S et al (2020) Review of rear emitter silicon heterojunction solar cells. Trans Electr Electron Mater 21(2):138–143. https://doi.org/10.1007/s42341-020-00172-5
27. Nogay G, Seif JP, Riesen Y et al (2016) Nanocrystalline silicon carrier collectors for silicon heterojunction solar cells and impact on low-temperature device characteristics. IEEE J Photovolt 6(6):1654–1662. https://doi.org/10.1109/JPHOTOV.2016.2604574
28. Lei C, Peng CW, Zhong J et al (2020) Phosphorus treatment to promote crystallinity of the microcrystalline silicon front contact layers for highly efficient heterojunction solar cells. Sol Energy Mater Sol Cells 209:110439. https://doi.org/10.1016/j.solmat.2020.110439
29. Ling ZP, Ge J, Mueller T et al (2012) Optimisation of p-doped µc-Si: H emitter layers in crystalline-amorphous silicon heterojunction solar cells. Energy Procedia 15:118–128. https://doi.org/10.1016/j.egypro.2012.02.014
30. Sharma M, Panigrahi J, Komarala VK (2021) Nanocrystalline silicon thin film growth and application for silicon heterojunction solar cells: a short review. Nanoscale Adv 3(12):3373–3383. https://doi.org/10.1039/d0na00791a
31. Green MA (1998) Solar cells: operating principles, technology, and system applications. University of New South Wales, Kensington
32. Zou S, Ye XY, Wu CK et al (2019) Complementary etching behavior of alkali, metal-catalyzed chemical, and post-etching of multicrystalline silicon wafers. Prog Photovolt Res Appl 27(6):511–519. https://doi.org/10.1002/pip.3125
33. Martini L, Serenelli L, Menchini F et al (2020) Silicon heterojunction solar cells toward higher fill factor. Prog Photovolt Res Appl 28(4):307–320. https://doi.org/10.1002/pip.3241
34. Schubert G (2006) Thick film metallisation of crystalline silicon solar cells: mechanisms, models and applications. University of Konstanz, Baden-Württemberg, Germany. https://www.semanticscholar.org/paper/cd60620c1e95b462500222f7b57b343eeb5de4cf
35. Rodofili A, Wolke W, Kroely L et al (2017) Laser transfer and firing of NiV seed layer for the metallization of silicon heterojunction solar cells by Cu-plating. Sol RRL 1(8):1700085. https://doi.org/10.1002/solr.201700085
36. Sun ZQ, Chen XQ, He YC et al (2022) Toward efficiency limits of crystalline silicon solar cells: recent progress in high-efficiency silicon heterojunction solar cells. Adv Energy Mater 12(23):2270094. https://doi.org/10.1002/aenm.202270094
37. Wenzel T, Lorenz A, Lohmüller E et al (2022) Progress with screen printed metallization of silicon solar cells—towards 20 µm line width and 20 mg silver laydown for PERC front side contacts. Sol Energy Mater Sol Cells 244:111804. https://doi.org/10.1016/j.solmat.2022.111804
38. Potts SJ, Phillips C, Jewell E et al (2020) High-speed imaging the effect of snap-off distance and squeegee speed on the ink transfer mechanism of screen-printed carbon pastes. J Coat Technol Res 17(2):447–459
39. Liang L, Li ZG, Cheng LK et al (2015) Microstructural characterization and current conduction mechanisms of front-side contact of n-type crystalline Si solar cells with Ag/Al pastes. J Appl Phys 117(21):215102. https://doi.org/10.1007/s11998-019-00291-6
40. Khanna A, Ling ZP, Shanmugam V et al (2013) Screen printed metallisation for silicon heterojunction solar cells. In: 28th European PV solar energy conference and exhibition. Villepinte, Frankreich, pp 1336–1339
41. Chen DP, Zhao L, Diao HW et al (2015) Choice of the low-temperature sintering Ag paste for a-Si: H/c-Si heterojunction solar cell based on characterizing the electrical performance. J Alloys Compd 618:357–365. https://doi.org/10.1016/j.jallcom.2014.08.175
42. Bai JG, Zhang ZZ, Calata JN et al (2005) Low-temperature sintering of nanoscale silver pastes for high-performance and highly-reliable device interconnection. In: Proceedings of ASME 2005 international mechanical engineering congress and exposition. Florida, pp 415–424. https://doi.org/10.1115/IMECE2005-79187
43. Schube J (2020) Metallization of silicon solar cells with passivating contacts. University of Freiburg, Baden-Württemberg
44. Kim MI, Choi EB, Lee JH (2020) Improved sinter-bonding properties of silver-coated copper flake paste in air by the addition of sub-micrometer silver-coated copper particles. J Mater Res Technol 9(6):16006–16017. https://doi.org/10.1016/j.jmrt.2020.11.069
45. Zhang RW, Lin W, Lawrence K et al (2010) Highly reliable, low cost, isotropically conductive adhesives filled with Ag-coated Cu

flakes for electronic packaging applications. Int J Adhesion Adhes 30(6):403–407. https://doi.org/10.1016/j.ijadhadh.2010.01.004
46. Körner S, Waltinger A, Partsch U et al (2016) High performance silver polymer pastes for SHJ cells.Publica.fraunhofer.de.https://publica.fraunhofer.de/starweb/servlet.starweb?path=epub0.web&search=N-421177
47. Li YM, Kim HS, Yi J et al (2018) Improved electrical performance of low-temperature-cured silver electrode for silicon heterojunction solar cells. IEEE J Photovolt 8(4):969–975. https://doi.org/10.1109/JPHOTOV.2018.2834955
48. Wang DL (2022) HJT low temperature metallization technology. In: 19th China photovoltaic academic conference, China
49. Chung K, Bang J, Thacharon A et al (2022) Non-oxidized bare copper nanoparticles with surface excess electrons in air. Nat Nanotechnol 17(3):285–291
50. Perelaer J, Smith PJ, Mager D et al (2010) Printed electronics: The challenges involved in printing devices, interconnects, and contacts based on inorganic materials. J Mater Chem 20(39):8446. https://doi.org/10.1039/c0jm00264j
51. Yongqiang X, Baojiao G, Jianfeng G (1997) The theory of thermodynamics for chemical reactions in dispersed heterogeneous systems. J Colloid Interface Sci 191(1):81–85
52. Wang B, Ji Z, Zimone FT et al (1997) A technique for sputter coating of ceramic reinforcement particles. Surf Coat Technol 91(1–2):64–68. https://doi.org/10.1016/S0257-8972(96)03115-5
53. Xu XR, Luo XJ, Zhuang HR et al (2003) Electroless silver coating on fine copper powder and its effects on oxidation resistance. Mater Lett 57(24–25):3987–3991. https://doi.org/10.1016/S0167-577X(03)00252-0
54. Chen KT, Ray D, Peng YH et al (2013) Preparation of Cu–Ag core-shell particles with their anti-oxidation and antibacterial properties. Curr Appl Phys 13(7):1496–1501. https://doi.org/10.1016/j.cap.2013.05.003
55. Zhang Q, Liang SH, Zhuo LC (2017) Fabrication and properties of the W-30wt%Cu gradient composite with W@WC core-shell structure. J Alloys Compd 708:796–803. https://doi.org/10.1016/j.jallcom.2017.03.064
56. Shin J, Kim H, Song KH et al (2015) Synthesis of silver-coated copper particles with thermal oxidation stability for a solar cell conductive paste. Chem Lett 44(9):1223–1225. https://doi.org/10.1246/cl.150424
57. Liu JH, Wang K, Yu FW et al (2020) A paste based on Cu@Sn@Ag particles for Die attachment under ambient atmosphere in power device packaging. J Mater Sci Mater Electron 31(3):1808–1816. https://doi.org/10.1007/s10854-019-02697-9
58. Sun HP, Wang KJ, Cai XL et al (2013) Preparation and performance of silver coated copper powder. Adv Mater Res 750–752:1057–1062. https://doi.org/10.4028/www.scientific.net/amr.750-752.1057
59. Schube J, Fellmeth T, Jahn M et al (2019) Advanced metallization with low silver consumption for silicon heterojunction solar cells. AIP Conf Proc 2156(1):020007. https://doi.org/10.1063/1.5125872
60. Hong W (2022) Research direction and progress of low-temperature paste for high-efficiency heterojunction cells. In: 19th China photovoltaic academic conference, China
61. Dhamrin M (2021) Low cost metallization approaches for advance solar cell structures. In: 17th China SoG Silicon and PV Power conference. Suzhou, China
62. Kim SY, Kim MI, Lee JH (2020) Pressure-assisted sinter-bonding characteristics at 250 ℃ in air using bimodal Ag-coated Cu particles. Electron Mater Lett 16(3):293–298. https://doi.org/10.1007/s13391-020-00208-1
63. Schneider A, Rubin L, Rubin G (2006) Solar cell efficiency improvement by new metallization techniques—the Day4 electrode concept. In: IEEE 4th world conference on photovoltaic energy conference. Waikoloa, HI, USA, pp 1095–1098. https://doi.org/10.1109/WCPEC.2006.279333
64. Faes A, Despeisse M, Levrat J et al (2014) SmartWire solar cell interconnection technology. In: Proceedings of the 29th European photovoltaic solar energy conference, Amsterdam, Niederlande, pp 2555–2561
65. Braun S, Micard G, Hahn G (2012) Solar cell improvement by using a multi busbar design as front electrode. Energy Procedia 27:227–233. https://doi.org/10.1016/j.egypro.2012.07.056
66. Zhao J, König M, Yao Y et al (2018) >24% silicon heterojunction solar cells on Meyer burger's on mass production tools and how wafer material impacts cell parameters. In: IEEE 7th world conference on photovoltaic energy conversion (WCPEC), Waikoloa, pp 1514–1519. https://doi.org/10.1109/PVSC.2018.8547908
67. Lossen J, Matusovsky M, Noy A et al (2015) Pattern transfer printing (PTP™) for c-Si solar cell metallization. Energy Procedia 67:156–162. https://doi.org/10.1016/j.egypro.2015.03.299
68. Adrian A, Rudolph D, Lossen J et al (2018) Benefits of pattern transfer printing method for finger metallization on silicon solar cells. In: Proceedings of the 35th European photovoltaic solar energy conference and exhibition, Brussels, pp 24–27
69. Mayberry R, Chandrasekaran V (2019) Metallization contributions, requirements, and effects related to pattern transfer printing (PTP™) on crystalline silicon solar cells. AIP Conf Proc 2156(1):020008. https://doi.org/10.1063/1.5125873
70. Geissbühler J, Faes A, Lachowicz A et al (2017) Metallization techniques and interconnection schemes for high efficiency silicon heterojunction PV. PV Tech (pv-tech.org). https://www.pv-tech.org/technical-papers/metallization-techniques-and-interconnection-schemes-for-high-efficiency-silicon-heterojunction-pv/
71. Tous L (2014) Nickel/copper plated contacts as an alternative to silver screen printing for the front side metallization of industrial high efficiency silicon solar cells. KU Leuven—Faculty of Engineering, Heverlee, Belgium
72. JBAO Technology Ltd. (2022) Patented copper electroplating equipment. www.jbao-tech.com, http://www.jbao-tech.com/Cn/ProductView, http://www.jbao-tech.com/Cn/ProductView.Accessed6June2022
73. Geissbühler J, de Wolf S, Faes A et al (2014) Silicon heterojunction solar cells with copper-plated grid electrodes: Status and comparison with silver thick-film techniques. IEEE J Photovolt 4(4):1055–1062. https://doi.org/10.1109/JPHOTOV.2014.2321663
74. Li ZT, Hsiao PC, Zhang W et al (2015) Patterning for plated heterojunction cells. Energy Procedia 67:76–83. https://doi.org/10.1016/j.egypro.2015.03.290
75. Yu J, Li JJ, Zhao YL et al (2021) Copper metallization of electrodes for silicon heterojunction solar cells: process, reliability and challenges. Sol Energy Mater Sol Cells 224:110993. https://doi.org/10.1016/j.solmat.2021.110993
76. Yu J, Bian JT, Liu YC et al (2017) Patterning and formation of copper electroplated contact for bifacial silicon hetero-junction solar cell. Sol Energy 146:44–49. https://doi.org/10.1016/j.solener.2017.02.022
77. Glatthaar M, Rohit R, Rodofili A et al (2017) Novel plating processes for silicon heterojunction solar cell metallization using a structured seed layer. IEEE J Photovolt 7(6):1569–1573. https://doi.org/10.1109/JPHOTOV.2017.2748999
78. Hatt T, Kluska S, Yamin M et al (2019) Native oxide barrier layer for selective electroplated metallization of silicon heterojunction solar cells. Sol RRL 3(6):1900006. https://doi.org/10.1002/solr.201900006
79. Hatt T, Mehta VP, Bartsch J et al (1999) (2018) Novel mask-less plating metallization route for bifacial silicon heterojunction solar

cells. AIP Conf Proc 1:040009. https://doi.org/10.1063/1.5049272
80. Adachi D, Terashita T, Uto T et al (2017) Effects of SiO_x barrier layer prepared by plasma-enhanced chemical vapor deposition on improvement of long-term reliability and production cost for Cu-plated amorphous Si/crystalline Si heterojunction solar cells. Sol Energy Mater Sol Cells 163:204–209. https://doi.org/10.1016/j.solmat.2016.12.029
81. Dabirian A, Lachowicz A, Schüttauf JW et al (2017) Metallization of Si heterojunction solar cells by nanosecond laser ablation and Ni–Cu plating. Sol Energy Mater Sol Cells 159:243–250. https://doi.org/10.1016/j.solmat.2016.09.021
82. Yu J, Zhang LP, Chen T et al (2019) Dual-function light-trapping: selective plating mask of SiO_x/SiN_x stacks for silicon heterojunction solar cells. Sol RRL 3(3):1800261. https://doi.org/10.1002/solr.201800261
83. Li JJ, Yu J, Chen T et al (2020) In-situ formation of indium seed layer for copper metallization of silicon heterojunction solar cells. Sol Energy Mater Sol Cells 204:110243. https://doi.org/10.1016/j.solmat.2019.110243

Shuai Zou is an assistant research fellow at the School of Physical Science and Technology, Soochow University, China. He earned his Ph.D. from Soochow University. He previously served as an associate R&D manager in the R&D department, Canadian Solar Inc., Suzhou. His research interests are focused on the fields of materials science and engineering, nanomaterials and their applications in photovoltaic devices, and nano biomaterials.

Xiaodong Su is a professor at the School of Physical Science and Technology, Soochow University, China. He earned his Ph.D. from Institute of Metal Research, Chinese Academy of Sciences. His research interests are focused on the fields of materials science and engineering, nanomaterials and their applications in photovoltaic devices, ferroelectric/magnetoelectrical functional materials and devices, and nano biomaterials.